



ELSEVIER

Physica D 74 (1994) 353–371

**PHYSICA** D

# Extreme sensitive dependence on parameters and initial conditions in spatio-temporal chaotic dynamical systems

Ying-Cheng Lai, Raimond L. Winslow

*Department of Biomedical Engineering, The Johns Hopkins University School of Medicine, Baltimore, MD 21205, USA*

Received 10 January 1994; revised 31 March 1994; accepted 1 April 1994

Communicated by K. Kaneko

## Abstract

We investigate the sensitive dependence of asymptotic attractors on both initial conditions and parameters in spatio-temporal chaotic dynamical systems. Our models of spatio-temporal systems are globally coupled two-dimensional maps and locally coupled ordinary differential equations. It is found that extreme sensitive dependence occurs commonly in both phase space and parameter space of these systems. That is, for an initial condition and/or a parameter value that leads to chaotic attractors, there are initial conditions and/or parameter values arbitrarily nearby that lead to nonchaotic attractors. This indicates the occurrence of an extreme type of fractal structure in both phase space and parameter space. A scaling exponent used to characterize extreme sensitive dependence on initial conditions and parameters is determined to be near zero in both phase space and parameter space. Accordingly, there is a significant probability of error in numerical computations intended to determine asymptotic attractors, regardless of the precision with which initial conditions or parameters are specified. Consequently, fundamental statistical properties of asymptotic attractors cannot be computed reliably for particular parameter values and initial conditions.

## 1. Introduction

Asymptotic attractors of dynamical systems are determined by both initial conditions and system parameters. In low-dimensional systems, sensitive dependence of asymptotic attractors on initial conditions can occur in systems that possess multiple attractors. Grebogi et al. first demonstrated that for some systems, basins of attraction are separated by fractal sets called fractal basin boundaries [1]. It is impossible to predict, with certainty, the asymptotic attractor for initial conditions in the neighborhood of fractal basin boundaries. Nonetheless, when ini-

tial conditions are away from these boundaries, one can still reliably predict the final asymptotic attractor. Systems with multiple attractors may also exhibit extreme types of fractal basins, the so-called “riddled basins” [2], in which at least one of the basins of attraction has the property that any neighborhood about each point within that basin contains points belonging to another basin. Finally, there can exist the so-called intermingled basin [2], in which all basins of attraction are riddled. Hence, for systems that exhibit riddled or intermingled basins, given any initial condition in these basins, it is impossible to predict the asymptotic attractor.

Dynamical systems may also exhibit sensitive dependence of their asymptotic attractors on parameters. This was first demonstrated by Farmer [3] using the one-dimensional quadratic map  $x_{n+1} = rx_n(1-x_n)$ . This map exhibits a unique attractor starting from almost all initial conditions in  $(0, 1)$  for any given value of the parameter  $r$  [4]. Attractors are of two types: chaotic and periodic. Farmer [3] demonstrated that the set of  $r$  values generating chaotic attractors (the chaotic parameter set) is a fractal set with positive Lebesgue measure [5] and box-counting dimension [6] one. Such sets have come to be known as “fat fractals” [3,7]. Most importantly, Farmer demonstrated that because of the fractal nature of the chaotic set, arbitrarily small perturbations  $\epsilon$  about parameter values  $r$  drawn from this set yield parameters  $r + \epsilon$  with non-zero probability of producing asymptotic attractors with completely different properties than those generated using parameter  $r$ .

To quantify sensitive parameter dependence, Farmer defined a so-called scaling exponent  $\beta$  [3,7,8]. This exponent was used to specify the measure of the set of “holes” in the fat fractal chaotic parameter set, *i.e.*, the set of  $r$  values that result in periodic attractors in the quadratic map above. Let  $h(\epsilon)$  be the total size of holes with width  $\geq \epsilon$ . Then the  $\epsilon$  coarse-grained measure of a fat fractal set can be defined as  $\mu(\epsilon) = 1 - h(\epsilon)/C$ , where  $C$  is the size of the parameter interval considered. For one-dimensional quadratic maps, Farmer conjectured that  $\mu(\epsilon)$  scales with  $\epsilon$  according to a power law in the limit of  $\epsilon \rightarrow 0$ ,

$$\mu(\epsilon) \sim \epsilon^\beta, \quad (1)$$

where  $\beta$  is the so-called fatness exponent [3]. For the quadratic map, Farmer found that  $\beta \approx 0.45$ .

Sensitive dependence of asymptotic attractors on both parameters and initial conditions can also be characterized using the uncertainty exponent first introduced by Grebogi et al. to quantify fractal basin boundaries [1]. They noticed

that  $\alpha$ , when used to characterize fat fractals, is equivalent to the exponent  $\beta$  [9]. The exponent  $\alpha$  can be calculated numerically as follows. Randomly choose a parameter value or an initial condition  $r_0$  in the fractal set. Define  $r' = r_0 + \epsilon$ , where  $\epsilon$  is a small perturbation. Determine whether the asymptotic dynamics of the system using these two parameters or two initial conditions are qualitatively different (chaotic versus periodic), in which case  $r_0$  is called an uncertain parameter value or an uncertain initial condition. Estimate the probability  $f(\epsilon)$  that  $r_0$  and  $r'$  yield different asymptotic dynamical behavior by repeating the experiment for many random choices of  $r_0$  in the parameter range or in the phase-space region of interest. Let  $N_u$  be the number of uncertain parameters or initial conditions among  $N_t$  randomly chosen parameter values or initial conditions at uncertainty  $\epsilon$ , then  $f(\epsilon) \approx N_u/N_t$ . In practice,  $f(\epsilon)$  decreases with decreasing  $\epsilon$ , typically scaling as  $f(\epsilon) \sim \epsilon^\alpha$  [1]. The uncertainty exponent is approximated by the slope of a straight line fit in a plot of  $\log_{10} f(\epsilon)$  versus  $\log_{10} \epsilon$ .

In numerical simulation of orbits,  $\epsilon$  can be viewed as the precision with which a parameter or an initial condition is specified. Then the scaling exponent  $\alpha$  determines the probability  $P(\epsilon)$  that the computed asymptotic behavior accurately reflects the true dynamics of the system. If  $\alpha > 1$ , reducing  $\epsilon$  can improve the probability of correct computation of the final state. If  $\alpha = 1$ , then improvement in  $\epsilon$  results in an equal improvement in the probability of correct computation of the final state. If  $\alpha < 1$ , then reduction of  $\epsilon$  will result in only a small reduction of  $P(\epsilon)$ . In particular, in the extreme case where  $\alpha \approx 0$  (e.g., riddled basins [2]), improvement in the precision  $\epsilon$  with which  $r$  is specified (even over many orders of magnitude) may result in only an incremental improvement in ability to predict the asymptotic state correctly.

For the logistic map, Grebogi et al. found that the uncertainty exponent  $\alpha$  is approximately 0.41 [1]. To appreciate the meaning

of  $\alpha = 0.41$ , assume that the parameter  $r$  can be determined to a precision of  $10^{-14}$ . Then  $P(\epsilon) \sim 10^{-6}$  and, hence, the probability of error in numerical prediction of the final state of the quadratic map is roughly one in one million. This means that computer simulations are generally reliable for this class of systems; we use the phrase “weak dependence” on parameters for such systems.

Investigations of phase space and parameter space sensitivities have been limited to low-dimensional chaotic systems. In this paper, we investigate extreme sensitivity to initial conditions and parameters in spatio-temporal chaotic dynamical systems. We study two classes of systems: (a) globally coupled Hénon map lattices (CMLs; [10–13]); and (b) locally coupled systems of ordinary differential equations (Duffing’s oscillators, [14]). Evidence will be presented of extreme sensitive dependence (characterized by near-zero uncertainty exponents) of asymptotic attractors on both initial conditions and parameters.

This paper is organized as follows. In Section 2, the system of globally coupled Hénon maps is introduced. Dynamics of this CML is investigated at different coupling strengths. In Section 3, we demonstrate that extreme sensitive dependence on parameters also occurs in locally coupled systems of differential equations. Conclusions and implications of these results to general spatio-temporal dynamical systems are presented in Section 4.

## 2. Globally coupled Hénon maps

### 2.1. CML equations and characterization of asymptotic attractors

The system of globally coupled Hénon maps can be expressed as follows:

$$x_{n+1}(i) = a - \left[ (1 - \delta)x_n(i) \right.$$

$$\left. + \frac{\delta}{N-1} \sum_{j,j \neq i}^N x_n(j) \right]^2 + by_n(i), \quad i = 1, \dots, N,$$

$$y_{n+1}(i) = x_n(i), \quad (2)$$

where  $i$  denotes discrete spatial sites,  $N$  is the total number of maps,  $n$  denotes iteration number,  $a$  and  $b$  are the parameters of the single Hénon map, and  $\delta$  is a parameter specifying coupling strength between maps at different site. The reason for choosing the Hénon map [15] is that it is one of the most extensively studied two-dimensional chaotic systems. (Locally coupled Hénon maps have been studied by Politi and Torcini [16].) For simplicity, we assume that each map couples to every other map with uniform coupling  $\delta$ . The determinant of the Jacobian matrix of the map is  $|DJ| = |(-b)^N|$  and, hence, for  $|b| < 1$  the system is highly dissipative. In the numerical computations to be described, we fix  $b = 0.3$ .

Asymptotic attractors can be characterized by the Lyapunov exponents of the system [17]. For  $N$  coupled two-dimensional maps, there are  $2N$  Lyapunov exponents. Let  $\lambda_1$  be the largest exponent, then  $\lambda_1 > 0$  indicates a chaotic attractor,  $\lambda_1 < 0$  indicates a periodic attractor, and  $\lambda_1 = 0$  signifies quasiperiodic motion. For a given set of parameters, we have used the algorithm by Benettin et al. [18] to compute the Lyapunov spectrum. The initial transient is chosen to be 10000 iterates. The precision for numerical determination of these exponents is set to  $10^{-7}$ , *i.e.*, the quantity  $\Delta\lambda_i = |\lambda_i(n+1) - \lambda_i(n)|$  is computed until  $\max\{\Delta\lambda_i\} \leq 10^{-7}$  ( $i = 1, \dots, 2N$ ), where  $n$  is the iteration number. The validity of the computed Lyapunov exponent spectrum is verified using the relation  $\sum_{i=1}^N \lambda_i = \log |DJ| = N \log |b|$ .

Figs. 1A and 1B show, for  $N = 10$  coupled maps, plots of  $\lambda_1$  and the number of positive Lyapunov exponents  $N_p$  versus the coupling strength  $\delta$ , respectively, where the parameter  $a$  is fixed at  $a = 1.4$  (it is believed that the single Hénon

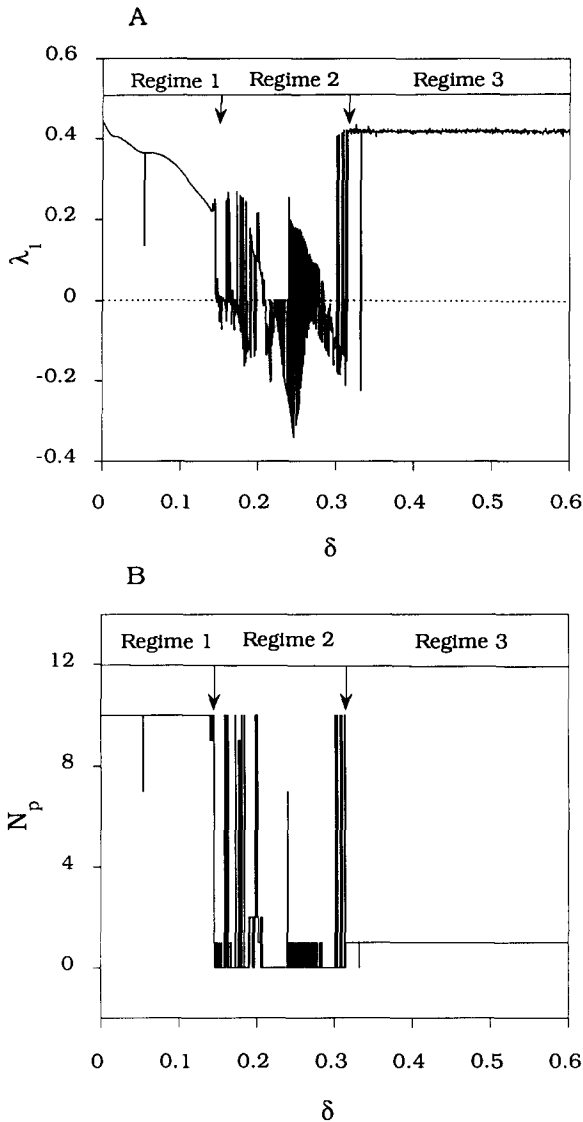


Fig. 1. Largest Lyapunov exponent  $\lambda_1$  (A), and number of positive Lyapunov exponents  $N_p$  (B) versus  $\delta$  (coupling strength) for a system of  $N = 10$  globally coupled Hénon maps with  $a = 1.4$  and  $b = 0.3$ . Three dynamical regimes are seen: (1) small  $\delta$  regime ( $\delta \leq 0.14$ ) where dynamical behavior of maps are nearly independent of each other; (2) moderate  $\delta$  regime ( $0.14 < \delta \leq 0.32$ ) in which the chaotic parameter set is riddled and there is an extreme sensitive parameter dependence; and (3) large  $\delta$  regime ( $\delta > 0.32$ ) where there is strong coherence among maps.

map has a chaotic attractor at this value of  $a$  when  $b = 0.3$ ). There are three distinct dynamic regimes as  $\delta$  is increased from 0. For most  $\delta$  values in regime 1 ( $0 < \delta \leq 0.14$ ),  $N_p = N$ , indicating that chaotic maps at each site behave independently. For most values of  $\delta$  within regime 3 ( $\delta > 0.32$ ), there is only one positive Lyapunov exponent, indicating the existence of a strong coherence among maps at different sites. An extremely sensitive parameter dependency occurs in regime 2 ( $0.14 < \delta \leq 0.32$ ), where large fluctuations in the values of both  $\lambda_1$  and  $N_p$  are observed as  $\delta$  is varied. The existence of these three distinct dynamic regimes is robust as  $N$ , the number of coupled maps, varies for Eq. (2). This was verified in our numerical studies for several  $N$  values (4, 20, 28 and 44).

## 2.2. Dynamics in the weakly coupling regime

Regime 1 is characterized by the existence of  $N$  positive Lyapunov exponents for a system of  $N$  coupled maps, as shown in Fig. 1B. Hence, in regime 1, maps evolve nearly independently of each other. Fig. 2 plots the Lyapunov spectra  $\lambda_i$  versus  $i$  ( $i = 1, 2, \dots, 2N$ ) at  $\delta = 0.1$ , where  $\lambda_1 \geq \lambda_2 \geq \dots \geq \lambda_{2N}$ , for  $N = 80$ . It is clear that there are  $N$  positive and  $N$  negative exponents with values close to 0.4 and -1.6 (the Lyapunov exponents of the single Hénon map). Therefore, the dynamics of individual maps in regime 1 can be described as independent.

Given this independence, it seems logical to assume that in regime 1, when each map is chaotic, the influence of the other  $N - 1$  maps on can be regarded as random noise [14]. In this case, the coupling term in Eq. (2) would be replaced by an additive random noise term. It has been established that small amplitude random noise can destroy the fine scale fractal structure of a chaotic attractor [19]. Specifically, for a single initial condition in the basin of attraction, the resulting asymptotic attractor computed from a large number of successive iterations no longer reveals any apparent fractal structure in

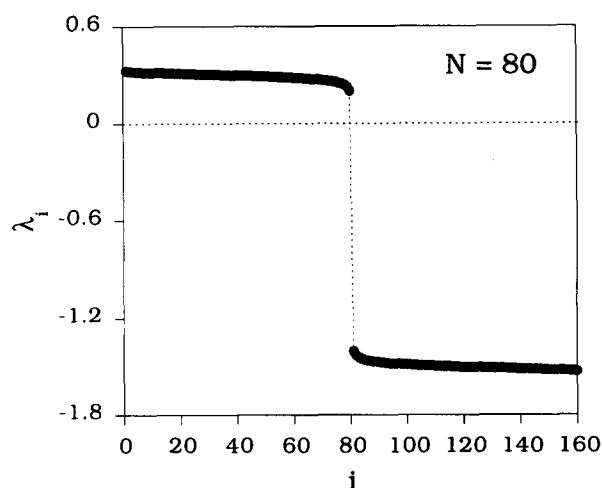


Fig. 2. Lyapunov spectra in the weakly coupled regime ( $\delta = 0.1$ ) at  $a = 1.4$  and  $b = 0.3$  for  $N = 80$ .

the presence of random noise. The attractor so recorded is usually a “fuzzy” attractor in the neighborhood of the original fractal attractor obtained in the absence of noise. We find that this result applies to the system of weakly coupled chaotic maps. Fig. 3A shows the chaotic attractor for the single Hénon map at  $a = 1.4$  and  $b = 0.3$ . Fig. 3B shows, when  $N = 10$  and  $\delta = 0.1$ , the attractor recorded at site  $i = 6$  for successive 6000 iterations (after discarding 20000 iterations of transient) from a single initial condition whose values of  $x_0(i)$  and  $y_0(i)$  ( $i = 1, 2, \dots, N$ ) were chosen randomly from  $[-2, 2]$ . Clearly, the attractor seen in Fig. 3B is a fuzzy version of Fig. 3A, indicating an influence similar to that of random noise from the remaining  $(N - 1) = 9$  maps. Attractors recorded from other sites exhibit similar features.

There is, however, a crucial difference between dynamics of weakly coupled chaotic maps and dynamics of low-dimensional chaotic system subject to small random noise. This is reflected in the structure of “snapshot” attractors computed for these systems. Snapshot attractors were originally introduced by Romeiras et al. [19] to study the fractal structure of chaotic attractors, including that of the single Hénon

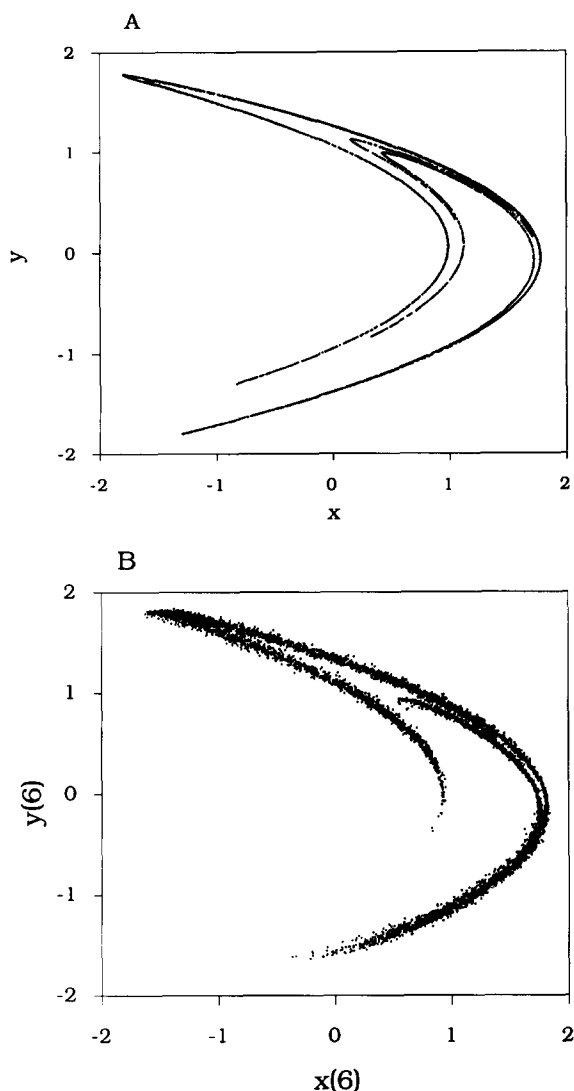


Fig. 3. (A) The chaotic attractor of the single Hénon map at  $a = 1.4$  and  $b = 0.3$ . (B) The attractor at site 6 of Eq. (2) at  $a = 1.4$ ,  $b = 0.3$ ,  $\delta = 0.1$  and  $N = 10$ . The attractor seen is a fuzzy version of that in (A) due to interactions among maps.

map, under the influence of random noise. The idea is that while the attractor recorded from a single initial condition over many iterations is fuzzy, fractal structure can still be revealed by evolving a large number of initial conditions simultaneously under the map for a long time, and then recording the images of all these initial conditions at an instant of time. The attractor

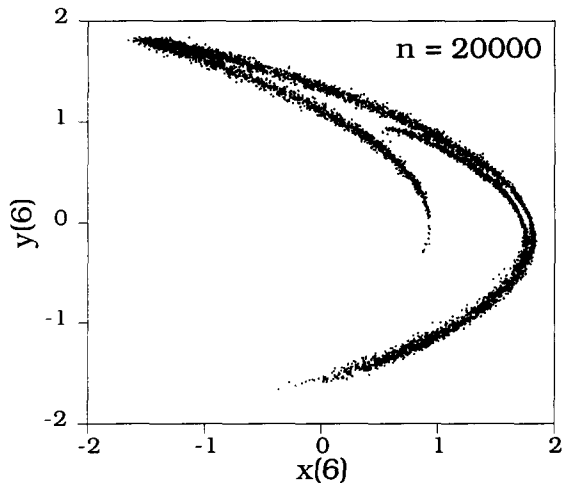


Fig. 4. For the same parameter setting in Fig. 3B, a snapshot attractor at site 6 at the 20000th iteration. The snapshot attractor was obtained by choosing a grid of  $80 \times 80$  initial conditions at site 6 in the region  $-2 \leq x(6) \leq 2$  and  $-2 \leq y(6) \leq 2$ , and iterating these 6400 initial conditions simultaneously under Eq. (2). Initial conditions at other sites are fixed as initial conditions in the  $x(6) - y(6)$  plane are varied. The snapshot attractor is fuzzy compared with the single Hénon attractor in Fig. 3A, indicating that weakly coupled maps have different dynamics from a single Hénon map subject to random noise.

so obtained is called a “snapshot attractor”. As time evolves, details of the snapshot attractor may change, but statistical properties of the snapshot attractor, such as multifractal dimension spectra, remain invariant at different instants of time [19]. For weakly coupled chaotic maps, we find that snapshot attractors recorded at different sites are also fuzzy and exhibit no apparent fractal structure. Fig. 4 shows a snapshot attractor for the same parameter setting as in Fig. 3B. To generate this attractor, 6400 initial conditions on site 6 were chosen uniformly from a  $80 \times 80$  grid in the two-dimensional region  $-2 \leq x_0(6) \leq 2$  and  $-2 \leq y_0(6) \leq 2$ , while initial conditions at other sites were fixed (chosen randomly initially). These initial conditions were then iterated forward simultaneously. The snapshot attractor determined at iterations  $n = 20000$  is shown. Similar to Fig. 3B, Fig. 4 reveals no evidence of sharp fractal structure

as seen in the single Hénon attractor (Fig. 3A). This observation thus suggests that dynamics of systems of weakly coupled chaotic maps are not equivalent to these of single individual maps with the coupling term replaced by an additive noise term.

When oscillating systems having distinct oscillation frequencies are coupled together, they can lock onto a common oscillating frequency even at low coupling values (see, for example, numerical studies of the dynamics of pacemaking cardiac cells [20]). This process is called frequency entrainment. Frequency entrainment also occurs in globally coupled Hénon maps. To demonstrate this, observe in regime 1 of Fig. 1A that there are rare values of  $\delta$  for which  $\lambda_1 < 0$ . At these  $\delta$  values, all Lyapunov exponents are negative, and attractors are stable periodic orbits. This is similar to the appearance of periodic windows interspersed within chaotic parameter regimes typically seen in low-dimensional systems such as the logistic map. Frequency entrainment usually occurs at these parameter values. Fig. 5A shows an example of frequency entrainment for  $N = 4$  coupled maps, where  $\delta = 0.1395$  ( $\lambda_1 = -0.125$ ). In Fig. 5A, the abscissa denotes time steps, and the ordinate plots values of all  $x(i)$ 's for  $i = 1, \dots, 4$ . Frequency entrainment is achieved at about 1825 iterations, after which all four maps evolve on a common period-4 orbit. To see that phases are different for different maps when frequency is entrained, Fig. 5B shows four time series at four sites (filled circles, filled diamonds, open circles, and open diamonds, respectively) for the parameter setting of Fig. 5A after a transient of 20000 iterations. Clearly, phases in all four maps are different, although they evolve on an identical stable period-4 orbit.

As the number of maps coupled in the system increases, clustering can occur in which maps form groups that evolve on different stable periodic orbits. Fig. 6 shows plots of the period of the asymptotic attractor (ordinate) versus the map site (abscissa) for  $N = 28$  and  $\delta = 0.0615$

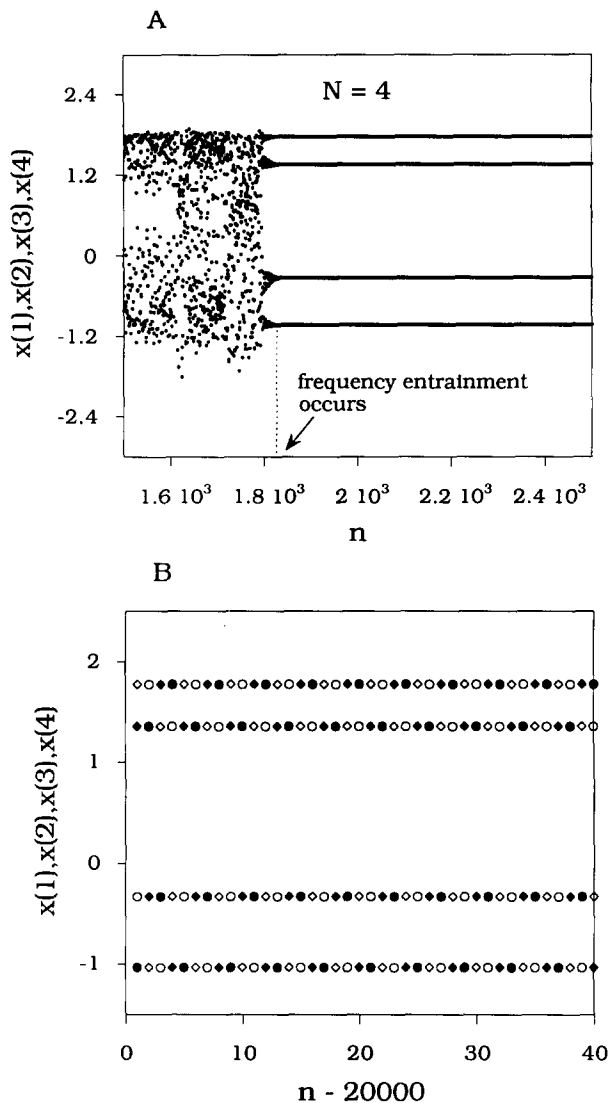


Fig. 5. (A) Frequency entrainment for coupled Hénon maps at  $a = 1.4$ ,  $b = 0.3$ ,  $\delta = 0.1395$  and  $N = 4$  where the largest Lyapunov exponent  $\lambda_1 \approx -0.125$ . Shown in the figure are four time series  $x(i)$ , where  $i = 1, 2, 3$  and  $4$  denote sites. (B) Part of the four time series represented by filled circles, filled diamonds, open circles and open diamonds, corresponding to the dynamical variable  $x$  at sites 1, 2, 3 and 4, respectively. Clearly, maps at four sites evolve on a common period-4 orbit but with different phases.

( $\lambda_1 = -0.066$ ). There are three distinct groups of clusters corresponding to different asymptotic stable periodic orbits. They are: period-7, period-14 and period-11. The phenomena of

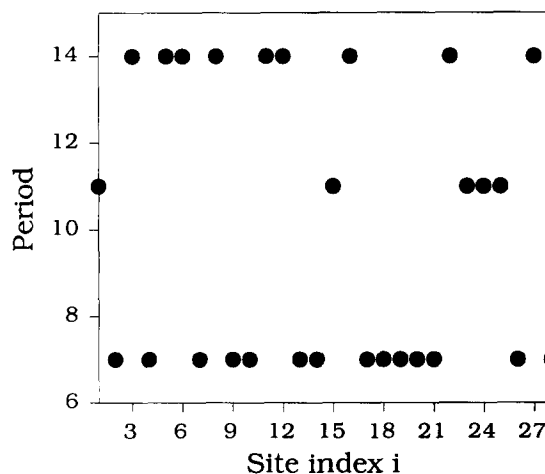


Fig. 6. Periods of stable orbits versus map site index for  $a = 1.4$ ,  $b = 0.3$ ,  $\delta = 0.0615$  and  $N = 28$ . Three distinct groups of maps are seen, whose attractors have period-7 (14 maps), period-11 (5 maps) and period-14 (9 maps), respectively.

both frequency entrainment and clustering have been previously studied in systems of coupled logistic maps by Kaneko [10,21].

Finally, we describe briefly the dynamics in the large coupling regime (regime 3). This regime is characterized by a presence of strong coherence among maps. For most values of coupling in this regime, there is only one positive Lyapunov exponent, as shown in Fig. 1B. This means that in regime 3, the dynamics of the whole system are similar to that of a single Hénon map.

### 2.3. Extreme sensitive dependence on initial conditions and parameters in the intermediate coupling regime

Dynamically, this regime is most interesting. There appear to be wild fluctuations of  $\lambda_1$  and  $N_p$  as  $\delta$  is varied. Analyses indicate that there are three types of asymptotic attractors in this regime: chaotic, quasiperiodic and periodic. When the asymptotic attractors are periodic, frequency entrainment and clustering can occur, similar to that shown in Figs. 5–6. Quasiperiodic

motion, characterized by  $\lambda_1 = 0$ , is also common in this regime. In such cases, asymptotic attractors are tori. We have observed that the occurrence of quasiperiodic motion appears to be more common when the number of coupled maps is small. For  $N = 4$  and  $a = 1.4$ , there even exists a continuous interval of  $\delta$  values in which  $\lambda_1 = 0$  so that every value of  $\delta$  leads to quasiperiodic motion, starting from randomly chosen initial conditions in phase space. This indicates that at fixed parameter values, the basins of these quasiperiodic attractors are large, and are unlikely to possess fractal structure. As  $N$  is increased, it is common that the basins of these attractors can be extremely complicated (fractals).

To detect multiple attractors and to study the structure of their basins, we fix a parameter value in regime 2 and compute the largest Lyapunov exponents  $\lambda_1$  for many different initial conditions. When  $N$  is large, the system is high dimensional and exploration of the entire phase space is difficult. We therefore take the following approach. We choose an arbitrary two-dimensional plane among  $2N$  variables and examine the type of attractors resulting from many initial conditions on this plane. A convenient choice is the plane defined by dynamical variables  $x(i)$  and  $y(i)$  at site  $i$ . Initial values of  $x(i)$  and  $y(i)$  are then varied systematically, while initial values of  $x(j)$  and  $y(j)$  ( $j = 1, \dots, N, j \neq i$ ) are held constant.

Fig. 7A shows, for  $N = 10$ ,  $a = 1.4$  and  $\delta = 0.245$ , a histogram of  $\lambda_1$  values resulting from 40000 initial conditions chosen at site 6 over a  $200 \times 200$  grid in the two-dimensional region  $-2 \leq x(6) \leq 2$  and  $-2 \leq y(6) \leq 2$ . There are three peaks at values of 0.18, 0, -0.32. This indicates the existence of three types of attractors: chaotic, quasiperiodic and periodic. Fig. 7B shows the projection of a chaotic attractor on the  $[x(6), y(6)]$  plane with  $\lambda_1 \approx 0.18$ . Figs. 7C–D show projections of a quasiperiodic and a period-4 attractor on the  $[x(6), y(6)]$  plane, respectively. Basins of these three types

of attractors are shown in Fig. 8, where red, blue and green dots denote basins of chaotic, quasiperiodic and periodic attractors, respectively. In most regions the basins of these attractors appear to be extremely intermingled. In these regions, for points that lead to chaotic attractors, there are points arbitrarily nearby that lead to nonchaotic attractors. This feature persists as successively smaller scales are examined. Fig. 9 shows a blowup of Fig. 8 in the region  $-0.49 \leq [x(6), y(6)] \leq -0.48$ , where the color coding is the same as in Fig. 8. Fig. 10A shows fractions of initial conditions leading to chaotic (filled circles), quasiperiodic (diamonds) and periodic (squares) attractors versus the size in the  $x(6)$ -direction of the two-dimensional region (logarithmic scale). These fractions are approximately constants at different phase space scales. Figs. 8, 9 and 10A thus strongly suggest that the basins of these attractors are fractal. To further quantify fractal basins, we have computed the uncertainty exponent  $\alpha$  [1] in phase space. The computation is performed by calculating  $\lambda_1$ 's for many initial conditions chosen on an arbitrary line segment in the  $[x(6), y(6)]$  plane. Fig. 10B plots the uncertain fraction versus perturbation on a base-10 logarithmic scale. The slope of the fitted straight line (an estimate of the uncertainty exponent) is  $0.024 \pm 0.005$ , a small value which is close to zero.

A near-zero uncertainty exponent in the phase space implies a similar exponent in parameter space. The reason is that for these extreme types of fractal basins, when a small change in the parameter occurs, there is a finite probability that the fine-scale structures of the fractal basins will be altered. Thus, even the same initial conditions under small parameter perturbation can give rise to completely different asymptotic attractors. More precisely, consider a dynamical system given by the following map that exhibits near-zero uncertainty-exponent fractal basins in phase space,

$$\mathbf{x}_{n+1} = \mathbf{F}(\mathbf{x}_n, \mathbf{p}), \quad (3)$$

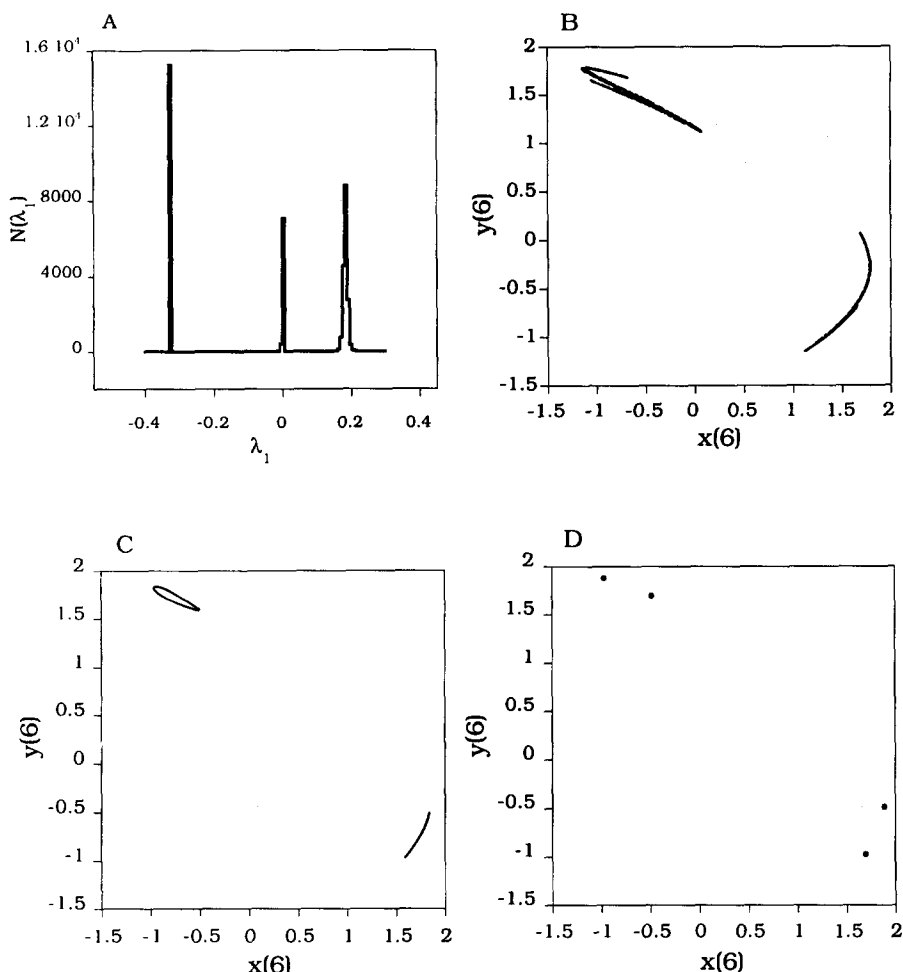


Fig. 7. (A) A histogram of largest Lyapunov exponents  $\lambda_1$  computed from 40000 initial conditions whose  $[x(6), y(6)]$  values are chosen uniformly on a  $200 \times 200$  grid defined over the region  $-2 \leq x(6), y(6) \leq 2$ . Parameter setting is  $a = 1.4$ ,  $b = 0.3$  and  $\delta = 0.245$  in Eq. (2). Three types of attractors are seen: chaotic ( $\lambda_1 \approx 0.18$ ) (B), quasiperiodic ( $\lambda_1 = 0$ ) (C) and periodic ( $\lambda_1 \approx -0.32$ ) (D).

where  $\mathbf{x} \in \mathbf{R}^n$  is the  $n$ -dimensional phase space variable, and  $\mathbf{p} \in \mathbf{R}^m$  denotes an  $m$ -dimensional parameter space. Assume that the initial condition  $\mathbf{x}_0$  and parameter value  $\mathbf{p}_0$  yield one type of asymptotic attractor. Extreme fractal basins mean that there is a finite probability that a perturbed initial condition  $\mathbf{x}'_0$  would yield a distinct type of attractor, where  $|\mathbf{x}'_0 - \mathbf{x}_0| \equiv |\Delta \mathbf{x}| \rightarrow 0$ . Using a Taylor expansion of  $\mathbf{F}(\mathbf{x}'_0, \mathbf{p}_0)$  at the point  $\mathbf{x}_0$  and  $\mathbf{p}_0$ , we have

$$\mathbf{F}(\mathbf{x}'_0, \mathbf{p}_0) = \mathbf{F}(\mathbf{x}_0, \mathbf{p}_0) + \mathbf{DF}_{\mathbf{x}}|_{\mathbf{x}_0, \mathbf{p}_0} \cdot \Delta \mathbf{x}, \quad (4)$$

where  $\mathbf{DF}_{\mathbf{x}}|_{\mathbf{x}_0, \mathbf{p}_0}$  is the  $n \times n$  Jacobian matrix with respect to  $\mathbf{x}$  evaluated at  $\mathbf{x}_0$  and  $\mathbf{p}_0$ . Alternatively, imagine that the term in Eq. (4) which is proportional to  $|\Delta \mathbf{x}|$  results from a small perturbation in the parameter space. We can then write

$$\begin{aligned} \mathbf{F}(\mathbf{x}'_0, \mathbf{p}_0) &\equiv \mathbf{F}(\mathbf{x}_0, \mathbf{p}_0) + \mathbf{DF}_{\mathbf{p}}|_{\mathbf{x}_0, \mathbf{p}_0} \cdot (\mathbf{p}'_0 - \mathbf{p}_0) \\ &= \mathbf{F}(\mathbf{x}_0, \mathbf{p}'_0), \end{aligned} \quad (5)$$

where  $\mathbf{DF}_{\mathbf{p}}|_{\mathbf{x}_0, \mathbf{p}_0}$  is the  $m \times m$  derivative matrix with respect to  $\mathbf{p}$  evaluated at  $\mathbf{x}_0$  and  $\mathbf{p}_0$ , and  $|\Delta \mathbf{p}| \equiv |\mathbf{p}'_0 - \mathbf{p}_0| \rightarrow 0$ . The parameter perturbation

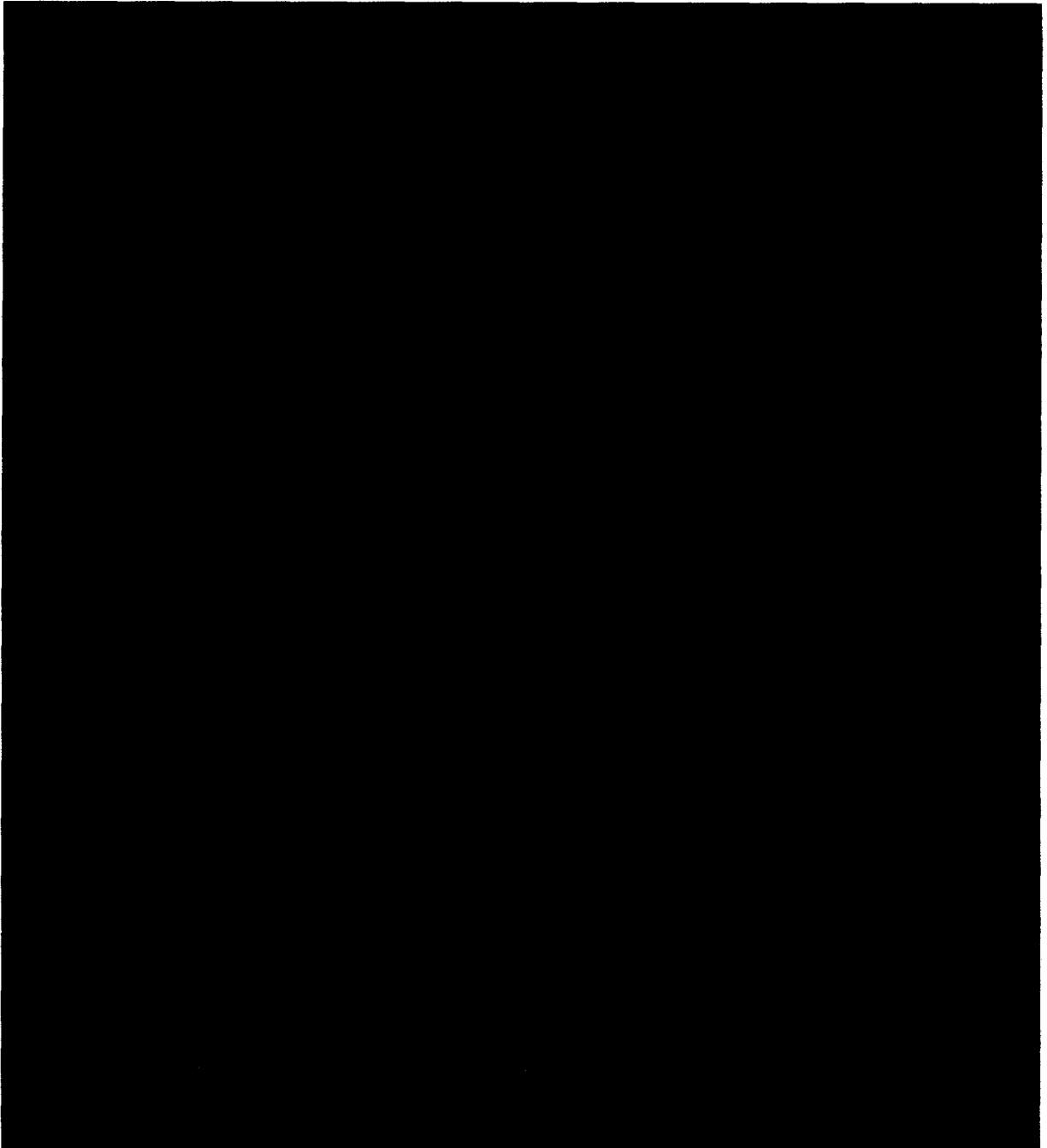


Fig. 8. Basins of chaotic (red), quasiperiodic (blue), periodic (green) attractors on  $[x(6), y(6)]$  plane in Fig. 7B–D, respectively.



Fig. 9. A blowup of Fig. 8 in the region  $-0.49 \leq [x(6), y(6)] \leq -0.48$ .

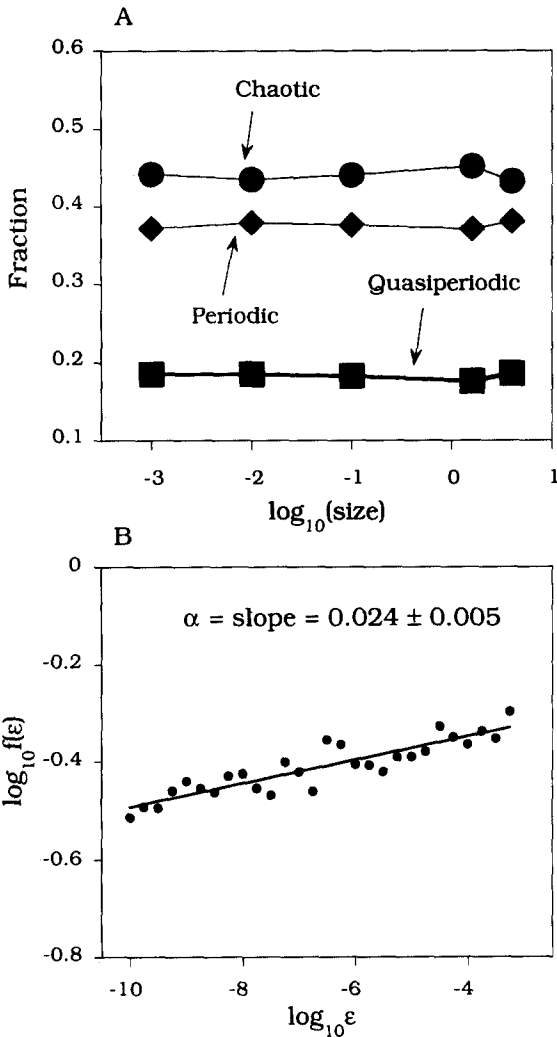


Fig. 10. (A) Fractions of initial conditions that lead to chaotic (diamonds), quasiperiodic (squares), and periodic (triangles) attractors versus the size of the square region from which a grid of  $200 \times 200$   $x(6)$  and  $y(6)$  values for initial conditions are chosen. Parameter settings are the same as in Fig. 7. (B) Plot of the fraction of uncertain initial conditions  $f(\epsilon)$  versus the uncertainty  $\epsilon$  on the base-10 logarithmic scale.

tion  $\Delta p$  is related to the perturbation in initial condition  $\Delta x$  by

$$DF_p|_{x_0, p_0} \cdot \Delta p = DF_x|_{x_0, p_0} \cdot \Delta x. \quad (6)$$

Eq. (6) indicates that behavior of the map  $F(x, p)$  under small changes in initial condition can be approximated by behavior under

small parameter changes, and vice versa. This implies that uncertainty exponents computed in both phase and parameter space are equivalent and, hence, an extreme sensitive dependence in phase space may imply extreme sensitive dependence in parameter space, and vice versa. This observation has been used previously to detect possible fractal basin boundaries in experimental settings [22].

To demonstrate fractal structure of parameter space, we examine a two-dimensional parameter space formed by  $a$  and  $\delta$ . Fig. 11A plots a chaotic parameter set in the  $(a, \delta)$  space for  $N = 10$ . This parameter space was sampled over a two-dimensional  $228 \times 460$  uniform grid in the parameter region  $1.0 \leq a \leq 1.4$  and  $0 \leq \delta \leq 0.35$ . The maximum Lyapunov exponent  $\lambda_1$  was computed at each grid point. In Fig. 11A, black dots denote parameter pairs for which  $\lambda_1 > 0$ , while white blank regions denote parameter regions of nonchaotic motion, *i.e.*,  $\lambda_1 \leq 0$ . Chaos occurs for  $a > 1.06$ . Clearly, there are regions of interspersed black and blank dots. Fig. 11B shows a blowup of part of Fig. 11A sampled over a  $300 \times 300$  uniform grid in the region  $1.35 \leq a \leq 1.4$  and  $0.2 \leq \delta \leq 0.25$ . Similar feature exists. This type of behavior persists on even much finer scales, as shown in Fig. 11C, which is an extended view of part of Fig. 11B in the region  $1.39 \leq a \leq 1.4$  and  $0.23 \leq \delta \leq 0.236$  sampled on a uniform  $300 \times 180$  grid. To see the fine scale fluctuation of  $\lambda_1$  in the parameter space, Fig. 12A plots, for  $N = 10$ ,  $\lambda_1$  versus  $\delta$  in  $0.245 \leq \delta \leq 0.248$  for fixed  $a = 1.4$ , where  $\lambda_1$ 's are computed for 600 values of  $\delta$  using identical initial conditions. These data thus suggest that for any random choice of the coupling parameter  $\delta$  in regime 2, an arbitrarily small perturbation about that value of  $\delta$  can give rise to completely different asymptotic dynamical behavior (e.g., a transition from chaos to periodic motion, or vice versa). Consequently, chaotic parameter sets in regime 2 are fractals (or are riddled) [23].

Fig. 12B shows a computation of the uncertainty exponent  $\alpha$  in the parameter space for

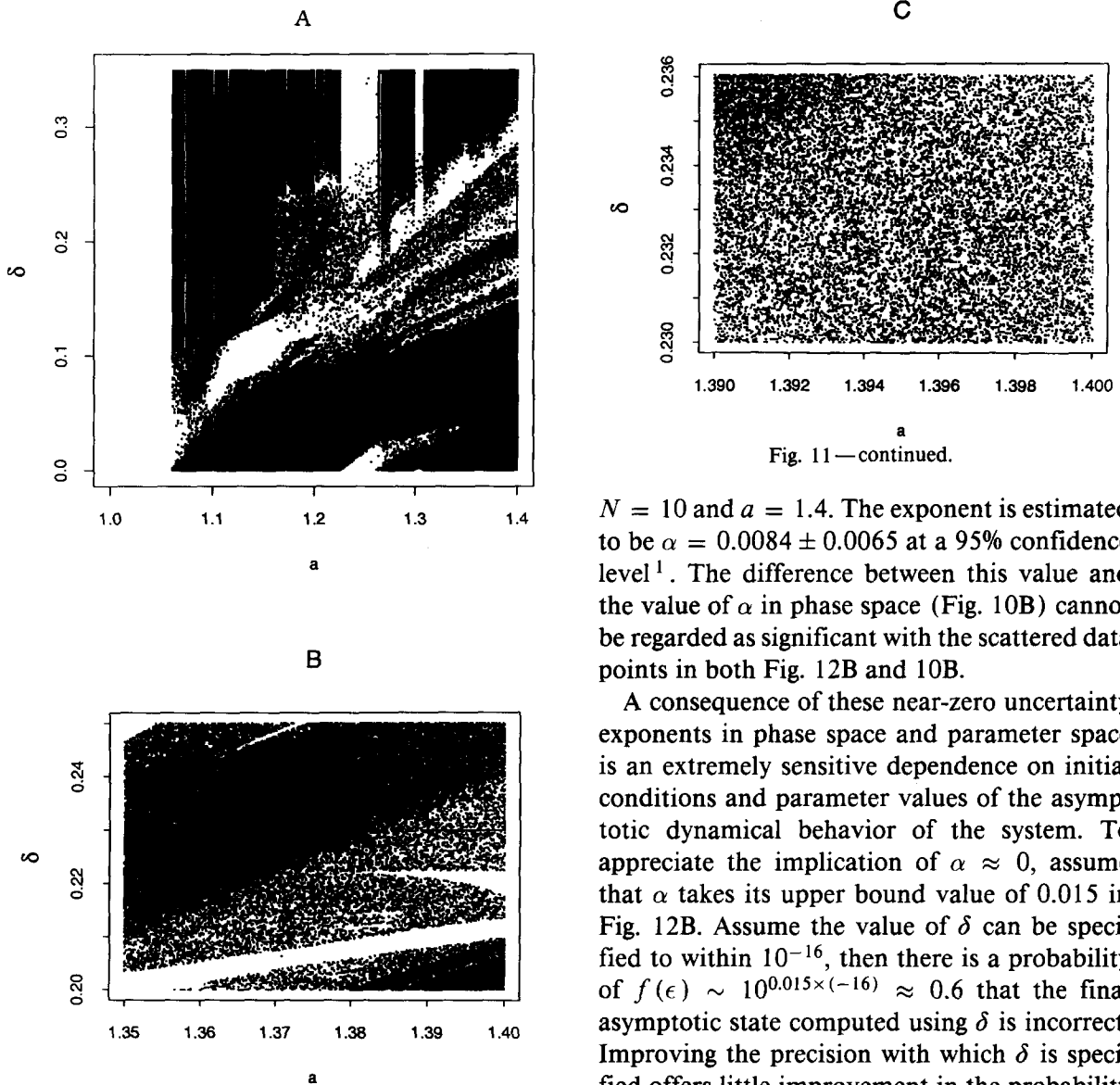


Fig. 11—continued.

$N = 10$  and  $a = 1.4$ . The exponent is estimated to be  $\alpha = 0.0084 \pm 0.0065$  at a 95% confidence level<sup>1</sup>. The difference between this value and the value of  $\alpha$  in phase space (Fig. 10B) cannot be regarded as significant with the scattered data points in both Fig. 12B and 10B.

A consequence of these near-zero uncertainty exponents in phase space and parameter space is an extremely sensitive dependence on initial conditions and parameter values of the asymptotic dynamical behavior of the system. To appreciate the implication of  $\alpha \approx 0$ , assume that  $\alpha$  takes its upper bound value of 0.015 in Fig. 12B. Assume the value of  $\delta$  can be specified to within  $10^{-16}$ , then there is a probability of  $f(\epsilon) \sim 10^{0.015 \times (-16)} \approx 0.6$  that the final asymptotic state computed using  $\delta$  is incorrect. Improving the precision with which  $\delta$  is specified offers little improvement in the probability

Fig. 11. (A) Values of parameters  $a$  and  $\delta$  that lead to chaotic attractor (black dots) and nonchaotic attractor (blank regions) in the two-dimensional parameter region  $1 \leq a \leq 1.4$  and  $0 \leq \delta \leq 0.35$  sampled over a uniform grid of  $228 \times 460$ . There exist regions in which black dots are interspersed with blank regions. For every black dot in these regions, there are blank regions arbitrarily nearby. Chaotic parameter sets in these interspersed regions are riddled. (B) A blowup of part of (A) over the region  $1.35 \leq a \leq 1.40$  and  $0.20 \leq \delta \leq 0.25$  uniformly sampled by a  $300 \times 300$  grid. (C) A blowup of part of (B) in  $1.39 \leq a \leq 1.40$  and  $0.230 \leq \delta \leq 0.260$  sampled by a uniform  $300 \times 180$  grid.

<sup>1</sup> The hypothesis that a fitted straight line has zero slope can be tested using linear regression theory [24]. In particular, for a linear fit  $y = \alpha x + b$ , there is a confidence interval  $[\alpha - k\sigma_y / \sqrt{(n-2)S_x^2}, \alpha + k\sigma_y / \sqrt{(n-2)S_x^2}]$  for the estimated slope  $\alpha$ , where  $\sigma_y$  is the standard deviation of the fit,  $S_x^2 = (1/n) \sum_i (x_i - \bar{x})^2$ ,  $n$  is the number of data points,  $\bar{x}$  is the averaged value of  $x_i$ , and  $k = \sqrt{F_{1-\gamma}(1, n-2)}$  (the  $F$ -distribution function, and  $1-\gamma$  is the confidence level). Typically,  $k$  increases with  $1-\gamma$ . If the confidence interval contains 0, then the hypothesis that  $\alpha = 0$  can be accepted with confidence level  $(1-\gamma)$  [24].

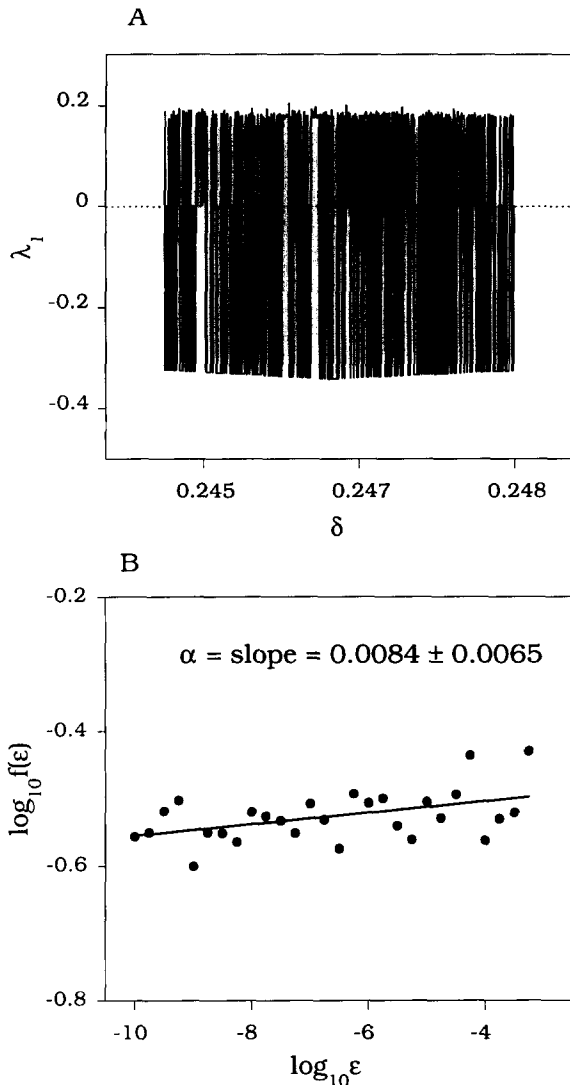


Fig. 12. (A) An expanded view of Fig. 1A in the parameter range  $0.248 \leq \delta \leq 0.249$ . (B) The uncertainty fraction  $f(\epsilon)$  computed using identical initial conditions versus the uncertainty  $\epsilon$  on the base-10 logarithmic scale. The uncertainty exponent is given by the slope of the straight line fit, which is estimated at a 95% confidence level to be  $0.0084 \pm 0.0065$ .

of computing the final state of the system correctly. For example, suppose computer precision is improved by 22 decades to  $10^{-38}$ . Then the probability of incorrectly computing the asymptotic state is still  $\approx 10^{0.015 \times (-38)} \approx 0.3$ , a small improvement in uncertainty with respect to the magnitude of the improvement in computer

precision. This indicates that computer calculation of the asymptotic state of the system in regime 2 cannot be reliable.

Such a small uncertainty exponent means that most values of  $\lambda_1$  computed within regime 2 are likely to be wrong, *i.e.*, positive value could be negative and vice versa (or chaos could be non-chaotic motion and vice versa). However, since there appears to be an approximately equal likelihood of counting a positive  $\lambda_1$  as negative, and for counting a negative  $\lambda_1$  as positive (Fig. 12A), the computation of the uncertainty fraction  $f(\epsilon)$  and the subsequent estimation of the uncertainty exponent  $\alpha$  from the data of Fig. 12B are reliable. This can be argued heuristically as follows. Note that the uncertainty fraction  $f(\epsilon)$  can be expressed as  $f(\epsilon) = N_u/N_t = N_u/(N_u + N_c)$ , where  $N_u$  is the number of uncertain parameter values, and  $N_c$  is the number of certain parameter values (parameter values that result in  $\lambda_1$  with same signs upon small perturbations). Let the uncertain probability at  $\epsilon$  be  $p$ , *i.e.*, the probability that  $\lambda_1 < 0$  (or  $> 0$ ) is  $p$  when it is numerically determined that  $\lambda_1 > 0$  (or  $< 0$ ). The errors in  $N_u$  and  $N_c$  are thus  $\Delta N_u = 2p(1-p)N_u$  and  $\Delta N_c = 2p(1-p)N_c$ , respectively. Therefore, to first order the error in  $f(\epsilon)$  is  $(N_c \Delta N_u - N_u \Delta N_c)/(N_c + N_u)^2 = 0$ .

As  $N$ , the number of coupled maps is increased, the features of Fig. 12 persist. Figs. 13A and 13B show, for  $N = 28$ , a plot of the largest Lyapunov exponent versus  $\delta$ , and the corresponding  $\log_{10} f(\epsilon)$  versus  $\log_{10}(\epsilon)$  plot computed for regime 2, respectively. The uncertainty exponent is estimated to be  $\alpha = 0.00066 \pm 0.0068$  at confidence level of 95%. When  $N = 44$ , We find that the uncertainty exponent is  $0.003 \pm 0.014$  at a 95% confidence level. Hence, for both  $N = 28$  and  $N = 44$ , the hypothesis that  $\alpha = 0$  cannot be rejected [24].

It can therefore be concluded that both the phase space and the parameter space of globally coupled Hénon maps exhibit an extreme type of fractal structure. Since these systems are simplified models of spatio-temporal dynamical

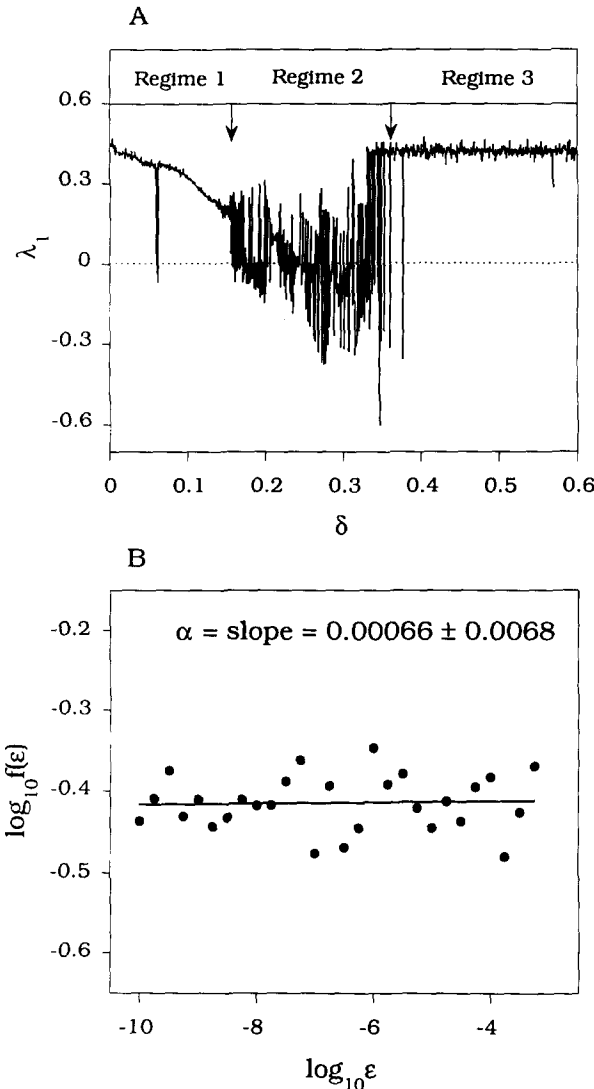


Fig. 13. (A) The largest Lyapunov exponent  $\lambda_1$  versus coupling  $\delta$  for  $N = 28$ ,  $a = 1.4$  and  $b = 0.3$ . (B) Plot of  $\log_{10}[f(\epsilon)]$  versus  $\log_{10}(\epsilon)$ . The uncertainty exponent is estimated at the 95% confidence level to be  $\alpha = 0.00066 \pm 0.0068$ .

systems, it is highly likely that the same type of sensitive initial condition and parameter dependence occurs in models of physical systems which are much more complicated than the model investigated in this paper.

### 3. Extreme sensitive dependence on parameters in locally coupled ordinary differential equations

In this Section we demonstrate that an extreme type of parameter dependence may also occur in the system of locally coupled Duffing's oscillators. The system can be expressed as follows:

$$\begin{aligned} \frac{dx^i(t)}{dt} &= y^i(t), \\ \frac{dy^i(t)}{dt} &= -\gamma \frac{dx^i(t)}{dt} - \sigma_1 [x^i(t)]^3 + \sigma_2 x^i(t) \\ &\quad + f \sin(\omega t) \\ &\quad + \delta [x^{i+1}(t) - 2x^i(t) + x^{i-1}(t)], \\ \frac{dz^i(t)}{dt} &= \omega, \quad i = 1, \dots, N. \end{aligned} \quad (7)$$

Without the coupling term  $\delta D_2[x^i(t)]$ , Eq. (7) is the well studied Duffing equation [22] which typically possesses chaotic attractors<sup>2</sup>. We consider the case where these oscillators are chaotic while uncoupled. A parameter setting for exhibiting chaotic attractor is  $\gamma = 1$ ,  $\sigma_1 = 100$ ,

<sup>2</sup> Eq. (7) can actually be derived from the following one-dimensional PDE that describes nonlinear wave propagation in forced, spatially extended medium with dispersion characterized by medium susceptibility  $\sigma_1$  and  $\sigma_2$ , and damping  $\gamma$

$$\frac{\partial^2 \Phi}{\partial t^2} = -\gamma \frac{\partial \Phi}{\partial t} - \sigma_1 \Phi^3 + \sigma_2 \Phi + \delta \frac{\partial^2 \Phi}{\partial z^2} + f \sin(\omega t), \quad (8)$$

where  $\Phi = \Phi(z, t)$  is the local displacement of the medium,  $\delta$  is a quantity that can be related to group velocity of the wave, and  $f$  is the forcing amplitude. Eq. (8) was first introduced by Umberger et al. [14]. To numerically solve Eq. (8) one first spatially discretizes it by substitutions  $z \rightarrow i$ ,  $\Phi(z, t) \rightarrow x^i(t)$  and  $\partial^2/\partial z^2 \rightarrow D_2 = x^{i+1} - 2x^i + x^{i-1}$ , where  $i$  is an integer denoting individual element at different spatial locations,  $x^i$  is the displacement at site  $i$ , and  $D_2$  is a discrete second-order differential operator. Eq. (8) thus becomes the following set of coupled ODEs:

$$\begin{aligned} \frac{d^2 x^i(t)}{dt^2} &= -\gamma \frac{dx^i(t)}{dt} - \sigma_1 (x^i(t))^3 + \sigma_2 x^i(t) \\ &\quad + f \sin(\omega t) + \delta D_2[x^i(t)], \quad i = 1, 2, \dots, N. \end{aligned} \quad (9)$$

Denote  $y^i(t) = dx^i(t)/dt$  and  $z^i(t) = \omega t$ , Eq. (9) is equivalent to Eq. (7).

$\sigma_2 = 10$ ,  $f = 1$  and  $\omega = 3.5$ . At this parameter setting, there is a chaotic attractor with  $\lambda_1 \approx 0.422$ .

In order to investigate parameter dependence of asymptotic attractors for the system of coupled Duffing's oscillators Eq. (7), it is necessary to compute  $\lambda_1$  for many different parameter values. Similar to our studies on CMLs, we vary the coupling strength  $\delta$ . The major difficulty is the amount of computation required. For  $N$  coupled oscillators, computing  $\lambda_1$  involves integrating  $6N$  first-order ODEs over many iterations. To make such a computation possible, we use the massively parallel Connection Machines CM5. Our strategy is to map Eq. (7) onto each processor of the CM5, and integrate these equations forward in time in parallel, assigning different local coupling values  $\delta$  to different processors. In this fashion,  $\lambda_1$  can be computed in parallel for many different  $\delta$  values. For each  $\delta$ ,  $\lambda_1$  is obtained by integrating Eq. (7) for 4000 iterations on the surface of section [defined by stroboscopic trajectories  $z^i(t) = 2\pi n$ , where  $n = 1, 2, \dots$ ] and then averaging  $\lambda_1$  over the last 400 iterations.

Fig. 14A plots  $\lambda_1$  versus  $\delta$  for  $0 < \delta < 20$  ( $N = 10$ , 2048  $\delta$  values) with identical initial conditions for all  $\delta$ . These data exhibit features similar to Figs. 1A and 13A. Specifically, there are three dynamic regimes. For most  $\delta$  values in regimes 1 and 3,  $\lambda_1$  varies rather smoothly with fluctuations determined by numerical uncertainties. In regime 2, there are significant fluctuations of  $\lambda_1$  whose amplitudes are at least one order of magnitude greater than the numerical uncertainties. The fluctuations in regime 2 therefore represent the dynamics of the system. This suggests the same type of extreme sensitive dependence of asymptotic attractors on  $\delta$  in regime 2, as described for the coupled Hénon maps. To see this qualitatively, Figs. 14B–C show two successive blowups of part of regime 2 for  $5.8 \leq \delta \leq 6.2$  (using 1024  $\delta$  values) and  $5.82 \leq \delta \leq 5.86$  (1024  $\delta$  values), respectively. It is clear that fluctuations of  $\lambda_1$  persist as smaller scales of pa-

rameter variation are examined. While no computation in the phase space and of the uncertainty exponents was attempted due to our limited source of CM5 usage, the similarity between Fig. 14 and Figs. 1A, 12–13A suggests that Eq. (7) exhibits extreme sensitive dependence in parameter space (and hence in phase space).

#### 4. Conclusions

In this paper, we have studied the dynamics of spatio-temporal chaotic systems described by systems of coupled maps and coupled differential equations. We have investigated extreme sensitivity of asymptotic attractors to both initial conditions and parameters. Our major findings can be summarized as follows.

- (i) It is common for these spatio-temporal systems to exhibit distinct multiple asymptotic attractors. Basins of attraction of these attractors can exhibit an extreme type of fractal behavior characterized by near-zero uncertainty exponents, which implies the same type of structure in the parameter space. The physical manifestation is that for almost every initial conditions in the phase space and/or for almost every parameter value in certain parameter regimes that asymptotes to one type of attractors, there are initial conditions and/or parameter values arbitrarily nearby that asymptote to other types of attractor.
- (ii) Fractal structures in phase space and parameter space indicate that asymptotic attractors in spatio-temporal chaotic systems are extremely unpredictable with respect to both initial conditions and parameters. Regardless of the precision with which initial conditions and parameters are specified, there is a significant error in computation of asymptotic attractors.

In general, chaos in low-dimensional dynamical systems is characterized by a sensitive dependence of system dynamic variables on initial

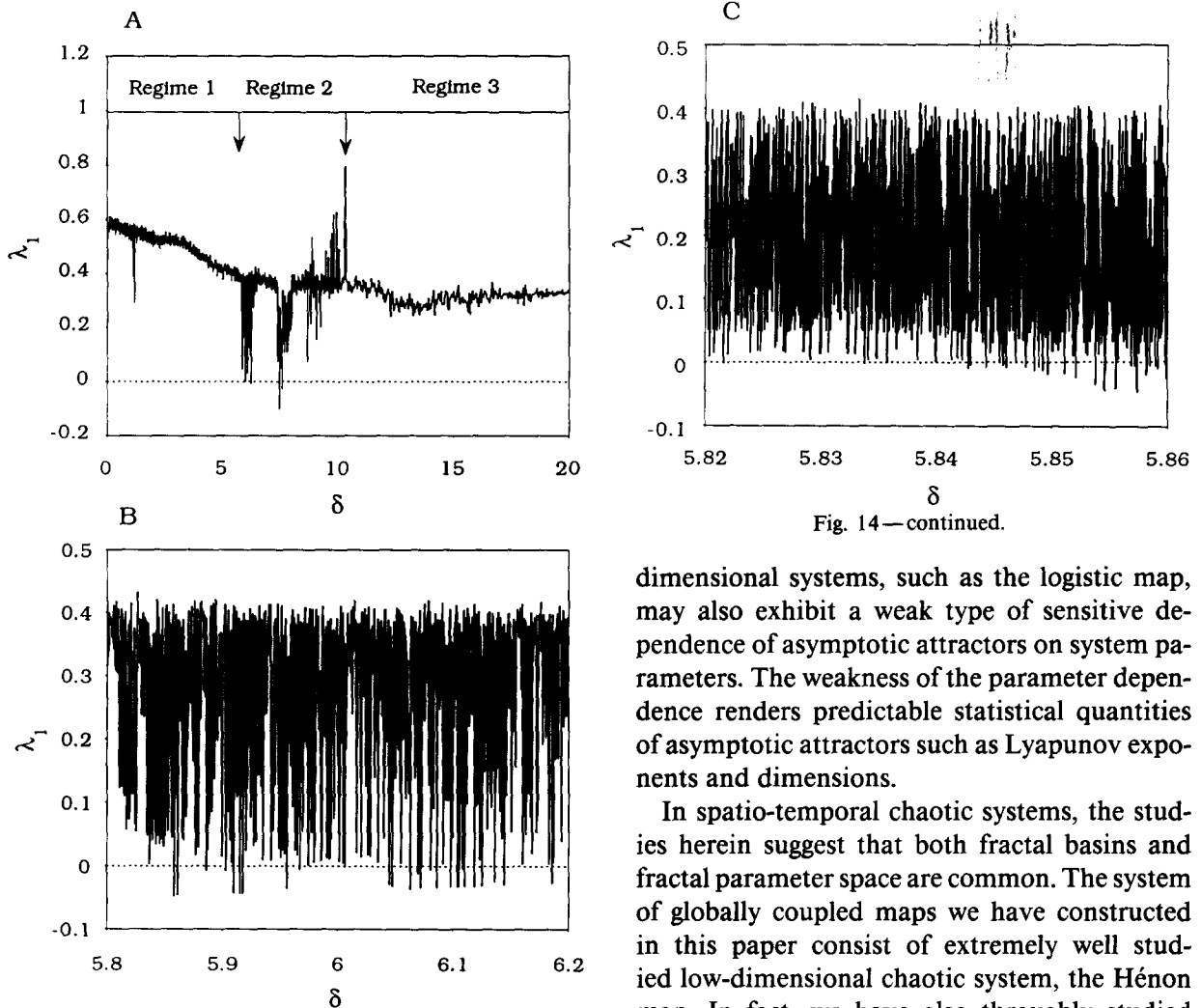


Fig. 14—continued.

Fig. 14. (A)  $\lambda_1$  versus  $\delta$  for the system of coupled Duffing oscillators Eq. (7) for  $0 \leq \delta \leq 20$  ( $N = 10$ , 2048  $\delta$  values). (B) An extended view part of regime 2 in (A) for  $5.8 \leq \delta \leq 6.2$  (1024  $\delta$  values). (C) An extended view of part of (B) for  $5.82 \leq \delta \leq 5.86$  (1024  $\delta$  values).

conditions in phase space ( $\lambda_1 > 0$ ). While the occurrence of extremely sensitive dependence on initial conditions has recently been discovered for low-dimensional systems whose phase spaces are riddled [2], it is also common that most low-dimensional chaotic systems do not exhibit such exotic phase space structures. For latter systems, it is still possible to predict, with certainty, the asymptotic attractors of the systems. Low-

dimensional systems, such as the logistic map, may also exhibit a weak type of sensitive dependence of asymptotic attractors on system parameters. The weakness of the parameter dependence renders predictable statistical quantities of asymptotic attractors such as Lyapunov exponents and dimensions.

In spatio-temporal chaotic systems, the studies herein suggest that both fractal basins and fractal parameter space are common. The system of globally coupled maps we have constructed in this paper consist of extremely well studied low-dimensional chaotic system, the Hénon map. In fact, we have also thoroughly studied the system of globally coupled Zaslavsky maps [25] and one of the most extensively studied spatio-temporal chaotic systems, the diffusively coupled logistic map lattices [10], and found similar phenomena. These three systems are, in fact, the only CML systems we have investigated in this study. Numerical evidence also indicates the existence of extreme sensitive parameter dependence in system of coupled ODEs. Thus, for spatio-temporal systems, there can be parameter regimes in which we cannot reliably predict the evolution of dynamic variables in phase space (since  $\lambda_1 > 0$ ), nor can we predict statistical properties of the asymptotic attractors for par-

ticular parameter values and initial conditions (since  $\alpha \approx 0$ ). This might provide insight to the fact that spatio-temporal chaotic systems are generally extremely unpredictable.

It is interesting that intuitively, one might expect spatio-temporal chaotic systems not to exhibit fractal basins. The reason is that the chaotic interaction among spatial elements may be modeled as random noise, and noise can wipe out the fine-scale structure of the system on a length scale determined by the coupling strength and, hence, one might expect arbitrarily fine fractal structures of basins to be smeared out [14]. Results of this paper in both the small and moderate coupling regimes suggest that this view may be incorrect. Weakly coupled spatio-temporal systems exhibit very different features (e.g., smeared snapshot attractors) from low-dimensional chaotic systems subject to random noise, while moderately coupled systems exhibit extreme types of fractal basins. The precise origin of these phenomena is still not clear. Intuitively, these phenomena may be attributed to the complicated interaction among elements at different spatial sites as a consequence of coupling.

Finally, we remark that extremely sensitive dependencies in both parameter space and phase space imply that spatio-temporal chaotic systems may be difficult to control. Recently, a successful controlling chaos strategy has been proposed for temporal chaotic systems [26]. The method makes use of arbitrarily small parameter perturbations to stabilize chaotic trajectories around some desired unstable periodic orbit embedded in chaotic attractors. The success of this method relies on dynamics' being smooth in the control parameter regime, namely, when small parameter perturbations are applied, it is required that no drastic change in asymptotic attractor occurs. For spatio-temporal chaotic systems, it is clear from the study of this paper that such a condition may well be violated. Arbitrarily small parameter perturbation may result in completely different asymptotic attrac-

tors. Hence, at present there is no assurance that spatio-temporal chaotic systems can be controlled.

### Acknowledgement

This work was supported by the National Institute of Health, Office of Naval Research, National Science Foundation and the Whitaker Foundation.

### References

- [1] C. Grebogi, S. W. McDonald, E. Ott and J. A. Yorke, *Phys. Lett. A* 99 (1983) 415; S. W. McDonald, C. Grebogi, E. Ott and J. A. Yorke, *Physica D* 17 (1985) 125.
- [2] J. C. Alexander, J. A. Yorke, Z. You and I. Kan, *Int. J. Bif. & Chaos* 2 (1992) 795; J. C. Sommerer and E. Ott, *Nature* 365 (1993) 138; E. Ott, J. C. Sommerer, J. C. Alexander, I. Kan and J. A. Yorke, *Phys. Rev. Lett.* 71 (1993) 4134.
- [3] J. D. Farmer, *Phys. Rev. Lett.* 55 (1985) 351.
- [4] D. Singer, *SIAM J. Appl. Math.* 35 (1978) 269.
- [5] M. V. Jacobson, *Comm. Math. Phys.* 81 (1981) 39.
- [6] J. D. Farmer, E. Ott and J. A. Yorke, *Physica D* 7 (1983) 153.
- [7] D. K. Umberger and J. D. Farmer, *Phys. Rev. Lett.* 55 (1985) 661.
- [8] R. Eykholt and D. K. Umberger, *Phys. Rev. Lett.* 57 (1986) 2333.
- [9] C. Grebogi, S. W. McDonald, E. Ott and J. A. Yorke, *Phys. Lett. A* 110 (1985) 1; C. Grebogi, E. Ott and J. A. Yorke, *Phys. Rev. Lett.* 56 (1986) 266.
- [10] K. Kaneko, *Prog. Theo. Phys.* 72 (1984) 480; 74 (1985) 1033.
- [11] K. Kaneko, ed., *Chaos* 2 (3), special issue on coupled map lattices, references therein.
- [12] K. Kaneko, *Phys. Rev. Lett.* 65 (1990) 1391; *Physica D* 54 (1991) 5; 55 (1992) 368.
- [13] S. Sinha, D. Biswas, M. Azam and S. V. Lawande, *Phys. Rev. A* 46 (1992) 3193; (1992) 6242; M. Ding and L. T. Wille, *Phys. Rev. E* 48 (1993) 1605.
- [14] D. K. Umberger, C. Grebogi, E. Ott and B. Afeyan, *Phys. Rev. A* 39 (1989) 4835.
- [15] M. Hénon, *Comm. Math. Phys.* 50 (1976) 69.
- [16] A. Politi and A. Torcini, *Chaos* 2 (1992) 293.
- [17] J.-P. Eckmann and D. Ruelle, *Rev. Mod. Phys.* 57 (1985) 617.
- [18] G. Benettin, L. Galgani, A. Giorgilli and J.-M. Strelcyn, *Meccanica* 15 (1980) 21.

- [19] F. J. Romeiras, C. Grebogi and E. Ott, *Phys. Rev. A* 41 (1990) 784.
- [20] D. Cai, R. Winslow and D. Noble, in: *Computer in Cardiology Proceedings* (IEEE Computer Society Press, New York, 1992);  
D. Cai, Y. C. Lai and R. L. Winslow, *Phys. Rev. Lett.* 71 (1993) 2501;  
A. Varghese and R. L. Winslow, *Physica D* 68 (1993) 364.
- [21] K. Kaneko, *Physica D* 34 (1989) 1; 37 (1989) 60.
- [22] F. C. Moon, *Phys. Rev. Lett.* 53 (1984) 962;  
F. C. Moon and G. -X. Li, *Phys. Rev. Lett.* 55 (1985) 1439.
- [23] Y. C. Lai and R. L. Winslow, *Phys. Rev. Lett.* 72 (1994) 1640.
- [24] B. W. Lindgren, *Statistical Theory* (Macmillan Pub. Co., New York, 1976);  
P. G. Hoel, S. C. Port and C. J. Stone, *Introduction to Statistical Theory* (Houghton Mifflin Co., Boston, 1971).
- [25] G. M. Zaslavsky, *Phys. Lett. A* 69 (1978) 145;  
L. Yu, E. Ott and Q. Chen, *Phys. Rev. Lett.* 65 (1990) 2935; *Physica D* 53 (1991) 102.
- [26] E. Ott, C. Grebogi and J. A. Yorke, *Phys. Rev. Lett.* 64 (1990) 1196.